

1 **Crop residue burning practices across north India inferred from** 2 **household survey data: bridging gaps in satellite observations**

3 Tianjia Liu¹, Loretta J. Mickley², Sukhwinder Singh^{3,4}, Meha Jain³, Ruth S. DeFries⁵, and
4 Miriam E. Marlier⁶

5 ¹Department of Earth and Planetary Sciences, Harvard University, Cambridge, MA, USA

6 ²School of Engineering and Applied Sciences, Harvard University, Cambridge, MA, USA

7 ³School for Environment and Sustainability, University of Michigan, Ann Arbor, MI, USA

8 ⁴Now at: Public Health Foundation of India, Gurgaon, India

9 ⁵Department of Ecology, Evolution, and Environmental Biology, Columbia University, New
10 York, NY, USA

11 ⁶Department of Environmental Health Sciences, University of California, Los Angeles, Los
12 Angeles, CA, USA

13 **Abstract**

14 In north India, agricultural burning adversely affects local and regional air quality during
15 the post-monsoon season (October to November), when the prevailing meteorology is favorable
16 for smog and haze formation. While the Moderate Resolution Imaging Spectroradiometer
17 (MODIS), aboard NASA's Terra and Aqua satellites, provides a nearly 20-year record of global
18 fire activity, the sensor cannot adequately capture small, short-lasting agricultural fires due to its
19 moderate spatial resolution (500 m to 1 km) and limited overpasses (twice daily for each
20 satellite), as well as the hazy conditions that typically obscure the north India land surface at this
21 time of year. Moreover, current global fire emissions inventories based on MODIS observations
22 can differ by up to an order of magnitude in this region. Here we incorporate household survey
23 data to bridge gaps in MODIS observations and calculate improved fire emissions over the states
24 of Punjab, Haryana, Uttar Pradesh, and Bihar during the 2003-2018 post-monsoon burning
25 seasons. We develop a method that adjusts MODIS Fire Radiative Power (FRP) for: (1)
26 additional small fires detected by the Visible Infrared Imaging Radiometer Suite (VIIRS) at 375-
27 m spatial resolution and (2) cloud/haze gaps in satellite observations; and (3) partial-field burns
28 and (4) the diurnal cycle of fire activity using household survey responses. Adjusting FRP for the
29 fire diurnal cycle yields the largest boost to emissions due to the short lifetime of the fires (~1/2
30 hour) and the brief windows of satellite detection. Using our adjusted FRP, we estimate on
31 average 10.8 Tg dry matter (DM) burned each year, yielding emissions of 68 Gg organic carbon
32 (OC), 5.8 Gg black carbon (BC), 821 Gg CO, and 15.4 Tg CO₂. On average, our OC+BC
33 emissions are ~250% higher than estimates from five widely used global fire emissions
34 inventories. Our estimate for Punjab, which contributes two-thirds of emissions in the region, is
35 consistent with our bottom-up validation using burn rates from the household survey and
36 government crop production statistics in 2016 and 2017. We spatially disaggregate the state-level
37 emissions to construct a gridded inventory at daily, 0.25° x 0.25° resolution over north India
38 from 2003-2018. Our inventory, SAGE-IGP (**S**urvey Constraints on FRP-based **A**gricultural Fire
39 **E**missions in the **I**ndo-**G**angetic **P**lain), can improve assessments of the impacts of agricultural
40 burning on air quality, public health, and regional climate, thus supporting effective policy

41 development to reduce these negative outcomes.

42 **1. Introduction**

43 Agricultural fires are an important seasonal source of outdoor emissions that degrade air
44 quality in north India (Liu *et al* 2018, Cusworth *et al* 2018, Vadrevu *et al* 2011). The practice of
45 agricultural burning in this region gained traction with the rise of combine harvester use in the
46 mid-to-late 1980s (Badarinath *et al* 2006, Liu *et al* 2019b). Mechanical harvesting generates
47 abundant root-bound and loose crop residues that are difficult to manage manually, and steady
48 increases in crop production have added to the volume of excess residues. For many farmers,
49 burning is a convenient, cost-effective method to remove crop residues and quickly transition
50 between the monsoon (*kharif*) and winter (*rabi*) crops. Recent bans and intervention efforts, such
51 as Happy Seeder technology, aim to reduce post-monsoon fires (Sidhu *et al* 2015, Tallis *et al*
52 2017, Shyamsundar *et al* 2019), which has increased by ~40-142% from 2003-2016 in the
53 western Indo-Gangetic Plain (IGP) (Liu *et al* 2019a, 2019b). Both satellites and ground-based
54 monitors have detected enhanced aerosol loading downwind of smoke plumes from agricultural
55 fires across north India in recent years (Badarinath *et al* 2009, Kaskaoutis *et al* 2014, Liu *et al*
56 2018, Jethva *et al* 2018, Sarkar *et al* 2018). Emission of gases and aerosols from open fires not
57 only degrades regional air quality and increases risk to acute respiratory infection and other lung
58 and cardiac diseases (Bikkina *et al* 2019, Chakrabarti *et al* 2019), but may also damage crops due
59 to elevated surface ozone exposure (Burney and Ramanathan 2014, Sinha *et al* 2015, Ghude *et al*
60 2016).

61 Much of the focus so far has been on agricultural fires in Punjab and Haryana, two
62 northern states that account for over 90% of post-monsoon fire intensity in India (Vadrevu *et al*
63 2013, Sarkar *et al* 2018, Liu *et al* 2019b). Less is known about burning practices elsewhere in
64 north India, such as Uttar Pradesh (UP) and Bihar, where many farmers also follow a rice-wheat
65 rotation (Singh *et al* 2011). This study examines crop residue burning practices in four states:
66 Punjab, Haryana, UP, and Bihar. One difficulty in monitoring agricultural fires in this region is
67 the coarse spatio-temporal resolution of satellite measurements (Liu *et al* 2019a). The small size
68 and duration of the fires, as well as increasing haziness from the smoke itself, also complicate
69 interpretation of satellite observations (Thumaty *et al* 2015, Cusworth *et al* 2018, Liu *et al*
70 2019a). These challenges may lead to gross underestimation of fire emissions driving
71 atmospheric models (Cusworth *et al* 2018, Dekker *et al* 2019). To date, such modeling studies
72 have relied on global fire emissions inventories due to the lack of inventories specific to India,
73 but emissions estimates, including those for aerosols, in the global inventories can differ by an
74 order of magnitude (Liu *et al* 2019a). Here we use survey data to help constrain satellite-based
75 estimates by filling observational gaps.

76 Our goals in this study are two-fold: (1) to use household survey data to improve
77 estimates of post-monsoon agricultural fire emissions and (2) to better understand the drivers,
78 consequences, and farmer perceptions of crop residue burning across north India. We develop a
79 FRP-based approach incorporating satellite and household survey data to adjust state-level
80 MODIS FRP for small fires from VIIRS, cloud/haze gaps in satellite observations, partial burns,
81 and the diurnal cycle in fire activity. We validate our FRP-based estimates using survey burn
82 rates, government statistics on crop production, and fuel-related factors from the literature.

83 Finally, we spatially disaggregate total dry matter (DM) burned to construct a daily, gridded
84 $0.25^\circ \times 0.25^\circ$ emissions inventory for Punjab, Haryana, UP, and Bihar from 2003-2018.

85 **2. Data and Methods**

86 *2.1 Study region*

87 Many agricultural regions across the Indian IGP are double-cropped with a rice-wheat
88 rotation, which is critical to the food security and livelihood of over 400 million inhabitants
89 across north India (Kumar *et al* 2015). In this study, we focus on four states in north India:
90 Punjab, Haryana, UP, and Bihar (Figure 1a). Punjab and Haryana, the western IGP states and
91 “breadbasket” of India, have ~ 1.5 times higher rice yields than UP and Bihar (Palanisami *et al*
92 2019).

93 *2.2 Household survey*

94 In a household survey in 2017, we asked over 2000 farmers in the four target states about
95 agricultural practices pertaining to rice harvests, burning of rice residues, and wheat sowing for
96 the 2016-17 growing season. For each village, we used a stratified purposive sampling technique
97 to select a subset of 20 households that represent the village-level distribution of landholding
98 sizes and social classes (Palinkas *et al* 2015). We hired two survey teams to conduct the surveys
99 on a mobile-based application in Hindi (Haryana, UP, and Bihar) and Punjabi (Punjab). In
100 particular, we asked farmers about the method of harvesting rice (mechanical or manual) and
101 subsequent burning of rice residues (Table S1). In 2018, we repeated the survey with 90% of the
102 same participants for the 2017-18 growing season and expanded our list of questions to
103 determine the farmers’ primary reasons for crop residue burning, as well as details on their
104 burning practices: (1) start year of burning, (2) method of burning (complete or partial burn of
105 field), (3) time of day for burning, (4) wait time (in days) from harvest to burning, and (5)
106 reasons for burning.

107 *2.3 Satellite datasets*

108 We use the MODIS Collection 6 gridded products for active fires
109 (MOD14A1/MYD14A1, 1 km), surface reflectance (MOD09GA/MYD09GA, 500 m), and land
110 cover (MCD12Q1, 500 m), all available from the Google Earth Engine platform (Gorelick *et al*
111 2017), to derive daily fire intensity and surface reflectance in agricultural regions across the IGP
112 (Table S6). We also use the higher spatial resolution active fire product (VNP14IMGML, 375m)
113 from the Visible Infrared Imaging Radiometer Suite (VIIRS), aboard the Suomi Near-Polar
114 Orbiting Partnership (S-NPP) and available from 2012.

115 As our fire metric, we rely on the daily maximum Fire Radiative Power (FRP), a proxy
116 for fire intensity. The Fire Radiative Energy (FRE), or the time integral of FRP, scales linearly to
117 dry matter burned (Wooster *et al* 2005).

118 Following Zhang *et al* (2014) and Liu *et al* (2019b), we estimate the start, midpoint, and
119 end of the cumulative FRP during each post-monsoon burning season from 2003-2018:

$$k_{\beta} = \arg \min_k \left[\left(\frac{\hat{y}_k}{\hat{y}_n} - \beta \right) > 0 \right], \text{ where} \quad (1)$$
$$\{k \mid k \in \mathbb{N}, 1 \leq k \leq n\}$$

where \hat{y}_k is the sigmoid-smoothed partial sums of the sequence of daily FRP over day 1 to k , n is the total number of days in the burning season, and k_{β} is the first day by when \hat{y}_k , normalized by the seasonal sum of FRP \hat{y}_n , has surpassed breakpoint β . We take $\beta = 0.1, 0.5$, and 0.9 to represent the start, midpoint, and end, respectively, of the burning season. Unlike Liu *et al* (2019b), here we test the effect of sigmoid smoothing on estimating β and its trends. For sigmoid smoothing, we use the nonlinear squares *nls* function in the R stats package to fit a sigmoidal curve to the partial sums of FRP:

$$\hat{y}_k = 1 / [1 + e^{a+bt}] \quad (2)$$

where a and b are shape parameters to be optimized and t is a sequence from 1 to n representing days in the burning season.

2.4 Statistical adjustments of agricultural fire emissions using satellite and survey data

Liu *et al* (2019a) found that MODIS cannot capture > 75% of small, short-lasting fires in Punjab and Haryana. While that study developed a hybrid MODIS-Landsat algorithm (ModL2T) to improve the spatial allocation of burned area (BA) and BA-based fire emissions, the low temporal resolution of Landsat (every 16 days) and the possible conflation of harvested area and burned area suggests that FRP-based algorithms may enable fire emissions estimates at finer temporal resolution and with lower commission errors. Here we first derive daily state-level post-monsoon fire emissions from 2003-2018 for Punjab, Haryana, UP, and Bihar from MODIS FRP (Sections 2.4.1-2.4.2). Then, we disaggregate the state-level emissions to a gridded, $0.25^{\circ} \times 0.25^{\circ}$ inventory (Section 2.4.3). We estimate emissions by state first rather than by grid cell to limit inconsistencies between neighboring grid cells and for computational efficiency.

2.4.1 Adjustment of FRP based on survey data and additional satellite observations

Using both satellite and household survey data, we adjust the MODIS FRP to account for small fires, cloud/haze gaps, partial burning, and limited satellite overpasses. For each state and year, we derive an adjusted daily FRP timeseries over a 4-month period, September to December. This extended study period for post-monsoon fires allows us to accommodate the different timing of each state's fire season and to ensure stability in smoothing FRP timeseries. Figure 2 shows the graphical depiction of each step detailed below.

1. MODIS observations of FRP. We first sum daily MODIS Terra and Aqua FRP during each post-monsoon burning season and over each state. This step assumes that the agricultural fires in this region are short-lived (~ 1/2 hour), following Thumaty *et al* (2015), and that the instruments detect different fires at the overpass times, Terra at 10:30 a.m. and Aqua at 1:30 p.m. Here we use the maximum FRP from the MOD/MYD14A1 gridded active fire product and apply an agricultural mask derived from MCD12Q1 to ensure that only cropland fires are considered. We adjust Terra and Aqua FRP separately for Steps 2-3 but sum the adjusted Terra and Aqua FRP at

157 the end of Step 3.

158 **2. Use of VIIRS observations for small fires.** Next, we incorporate the FRP observations from
159 VIIRS, which at 375 m has a finer spatial resolution than the MODIS products (1 km) and so can
160 more accurately capture fine-scale fire activity than MODIS. To account for these missing small
161 fires, we diagnose those VIIRS active fires that do not intersect with MODIS/Aqua active fires
162 within a 1-km buffer and then add VIIRS FRP of these fires to MODIS/Aqua FRP. We use only
163 MODIS/Aqua FRP because VIIRS does not observe active fires during the MODIS/Terra
164 overpass. Because VIIRS observations are available only from 2012-2018, we derive the
165 incremental VIIRS boost for 2003-2011 for the entire state by taking the average ratio of
166 additional VIIRS FRP and MODIS/Aqua FRP over 2012-2018 and then scaling up the
167 MODIS/Aqua FRP over the earlier years by that ratio. We also boost MODIS/Terra FRP
168 uniformly by the same ratio from 2003-2018 to account for missed small fires during the
169 morning overpass.

170 **3. Filling in gaps of observed FRP due to clouds and haze.** The evolution of fire activity over
171 the burning season as detected by MODIS is not smoothly varying but is instead characterized by
172 dips or gaps in regional total FRP. Cusworth *et al* (2018) suggest that this large day-to-day
173 variability in FRP is due in large part to clouds, haze, and/or smoke, occasionally obscuring the
174 fire activity on the ground. To test this hypothesis, we check whether these dips or gaps in the
175 summed FRP timeseries for each state correspond with MODIS observations of surface
176 reflectance (MOD/MYD09GA) in the red visible band, ρ_1 . As noted above, surface reflectance
177 in this band is sensitive to clouds or haze and so would be expected to anticorrelate with the area
178 within which satellites can “see” fires during the burning season. We then take advantage of ρ_1
179 measurements to gauge the extent to which clouds or haze interferes with fire detection, and we
180 iteratively fill in the cloud/haze gaps in the statewide data for each fire season. Additional details
181 on cloud/haze gap filling procedure is described in [Supplementary Section S3.2](#).

182 **4. Boosting FRP with survey data on partial burning.** The survey data reveal that in the four
183 states, 30-57% of farmers piled the loose crop residue in the center of the field before setting the
184 residue on fire, resulting in partial burning of the field. Taking the practice into account has
185 importance in constructing fire emission inventories for three reasons. First, partial burns,
186 covering small, discrete areas, are less likely to be observed from space than complete burns (Liu
187 *et al* 2019a). Second, only loose residues are set on fire in partial burns, yielding less DM burned
188 than in complete burns (Kumar *et al* 2015). Third, the PM_{2.5} emissions factor, with respect to the
189 mass of rice residue burned, has been observed in partial burns to be on average ~1.92 times that
190 for complete burns due to the incomplete, smoldering combustion of wetter residues (Lasko and
191 Vadrevu 2018).

192 To overcome these challenges, we assume as an upper bound that all partial fires have been
193 missed by satellite detection (Liu *et al* 2019a). For each state, we boost the daily FRP by the
194 partial-burn fraction derived from survey data and normalized by operational landholding area.
195 To account for the lower mass of DM burned in partial burns, we also apply a scaling factor to
196 the partial-burn FRP, since FRP is linearly proportional to DM burned (Wooster *et al* 2005).
197 Here we scale partial-burn FRP by 0.75, or the approximate fraction of total crop residues that
198 are piled in the center of the field and burned. This factor assumes a rice plant height of ~101 cm
199 (Mahajan *et al* 2009), of which 20-22 cm are left standing after harvest (Mahajan *et al* 2009).

200 Our resulting estimates of FRP from partial fires are then distributed uniformly in time across
201 each burning season.

202 **5. Adjustment to take into account the diurnal cycle of fire activity.** The two satellites
203 associated with MODIS each have one daytime overpass per day – Terra at 10:30 a.m. and Aqua
204 at 1:30 p.m. Typically, Aqua detects over five times as many fires as Terra in northwest India
205 during the post-monsoon (Liu *et al* 2019a). These overpass times can miss the peak burning
206 times of individual agricultural fires, which are small and short-lived, each lasting only about
207 half an hour (Thumaty *et al* 2015). Here we adjust the satellite-derived FRP to reflect those fires
208 unseen by satellites. We also take advantage of the survey data to adjust the FRP captured by
209 MODIS to reflect the diurnal variation of agricultural fire activity, separated into four time
210 periods: early morning (4-10 a.m.), mid-day (10 a.m.-2 p.m.), evening (2-6 p.m.), and late night
211 (6-11 p.m.). For example, the survey data reveal that 8-41% of IGP farmers typically set fires
212 between 10 a.m.-2 p.m., depending on the state. Additionally, the Terra and Aqua/S-NPP
213 daytime overpasses only partly overlap with the mid-day burning window, assuming that all fires
214 last half an hour. Accounting for variance in when satellites see each fire and how long each fire
215 burns, we estimate that satellite-derived FRP captures just ~1.5 hours of fire activity over this 4-
216 hr mid-day time interval. To correct for this discrepancy, we take the total mid-day FRP as 2.67
217 times the satellite-derived FRP. This 2.67 factor assumes linearly increasing FRP from the Terra
218 to Aqua overpass over 45-minute blocks during the 4-hr mid-day window. We further adjust
219 daily total FRP by assuming that all fires outside the mid-day window are undetected and by
220 adding FRP increments according to the temporal distribution implied by the survey data. We
221 weight these increments by the operational landholding area with reported burning in each time
222 window.

223 As a post-processing step, we remove anomalous FRP spikes that often occur outside the
224 burning season and are likely contaminated by false satellite detections. An anomalous day is
225 tagged if its FRP exceeds three times the maximum FRP in a 2-day buffer window (4 days in
226 total) and is above the 25th percentile of daily FRP from September-December of that year.

227 To account for agricultural fires that extend eastward from Haryana into the state of
228 Rajasthan along the Ghaggar-Hakra River, we also include Ganganagar and Hanumangarh, two
229 districts in north Rajasthan. We follow the same methods as described above but use survey data
230 from Haryana for Steps 4-5.

231 2.4.2 Conversion to dry matter burned and emissions

232 For the final step in constructing our improved fire inventory, we follow Kaiser *et al*
233 (2012) to convert FRP in each grid cell to dry matter burned and then to emissions for various
234 chemical species, as is done in constructing the Global Fire Assimilation System (GFAS)
235 emissions inventory:

$$236 \quad E_i = FRE \times \alpha \times EF_i \quad (3)$$

237 where E_i is the emissions of species i (g species), FRE is the fire radiative energy (MJ), or the
238 time integral of FRP, α is a conversion factor dependent on land use/land cover (kg DM MJ⁻¹)
239 that yields DM burned, and EF_i is the emissions factor for species i (g species kg⁻¹ DM). To
240 convert FRP to FRE, we multiply the adjusted daily FRP by the lifetime of the agricultural fires,

241 which we assume to be 30 minutes, or $1.8 \times 10^4 \text{ s day}^{-1}$, in this region (Thumaty *et al* 2015).
242 Following Kaiser *et al* (2014) and Liu *et al* (2015), we use a conversion factor α for agricultural
243 fires of 0.41 kg MJ^{-1} .

244 To validate the DM burned derived from adjusted FRP, we focus on Punjab, which
245 accounts for $> 85\%$ of MODIS-observed FRP during the post-monsoon in the study region. We
246 use a bottom-up method, following Aalde *et al* (2006), that involves burn rates from the
247 household survey and government crop production estimates from the Indiastat data portal
248 (Indiastat.com), and crop-specific parameters from literature for 2016 and 2017:

$$249 \quad E_i = f_{burned} \times CP \times RC \times f_{DM} \times f_{CC} \times EF_i \quad (4)$$

250 where f_{burned} is the fraction burned, CP is crop production in kg (in this case, of *kharif* rice), RC
251 is residue-to-crop ratio, f_{CC} is combustion completeness, and f_{DM} is the mass fraction of DM
252 burned of total from crop production (Table 1). Here, fuel loading (FL) is the product of CP , RC ,
253 and f_{DM} over the cultivated area (A) in units of g m^{-2} ; fuel consumption (FC) is the product of
254 fuel loading and f_{CC} :

$$255 \quad FL = \frac{CP \times RC \times f_{DM}}{A} \quad (5)$$

$$256 \quad FC = FL \times f_{CC} \quad (6)$$

257 We also consider the IPCC recommended fuel load of 550 g m^{-2} for rice residues (Aalde *et al*
258 2006). Following the FRP-based method for estimating adjusted DM burned, here we also adjust
259 the DM for partial burns using survey data.

260 As we will see, our top-down estimates of fuel load agree well with bottom-up validation
261 for the 2016 and 2017 post-monsoon burning seasons (Section 3.2). We then extend these
262 bottom-up estimates to 2003-2018 by first calculating the ratio of survey burn rates to the
263 satellite-derived, adjusted FRP for 2016-17 and then applying this ratio to all years in the satellite
264 FRP record.

265 Finally, application of emissions factors from Andreae (2019) allows us to quantify
266 emissions of black carbon (BC) and primary organic carbon (OC), as well as of CO_2 and CO ,
267 from the agricultural fires. For OC and BC from partial burns, we additionally scale DM by a
268 factor of 1.92 to account for the higher $\text{PM}_{2.5}$ emissions factor in these fires relative to complete
269 burns (Lasko and Vadrevu 2018), as described in Section 2.4.1. We compare the resulting
270 statewide emissions estimates with five global inventories: (1) Global Fire Emissions Database
271 (GFEDv4s; van der Werf *et al* 2017), (2) Fire Inventory from NCAR (FINNv1.5; Wiedinmyer *et*
272 *al* 2014), (3) Global Fire Assimilation System (GFASv1.2; Kaiser *et al* 2012), (4) Quick Fire
273 Emissions Dataset (QFEDv2.5r1; Darmenov and da Silva 2013), and (5) Fire Energetics and
274 Emissions Research (FEERv1.0-G1.2; Ichoku and Ellison 2014). GFEDv4s and FINNv1.5 are
275 primarily derived from burned area (BA) and active fire area (AFA), while GFASv1.2,
276 QFEDv2.5r1, and FEERv1.0-G1.2 are FRP-based. More details about these inventories are given
277 in Supplementary Sections S4.1-4.2.

278 2.4.3 Constructing a spatially and temporally explicit gridded emissions inventory

279 The steps described so far yield total seasonal emissions for each state for 2003-2018. We
280 next disaggregate the state-level DM emissions to daily, $0.25^\circ \times 0.25^\circ$ spatial resolution to create
281 a gridded inventory, SAGE-IGP. We start with total state-level emissions rather than the finer
282 gridded resolution to limit noise and ensure convergence in our cloud/haze gap-filling step and to
283 aggregate survey responses from sparsely located households.

284 First, we allocate the seasonal DM emissions spatially according to the fraction of
285 MODIS Terra + Aqua unadjusted FRP in each grid cell for the season. Second, we approximate
286 the evolution of fire activity over the season in each grid cell as Gaussian, using the dates of
287 three breakpoints, or k , where $\beta = 0.1, 0.5$, and 0.9 (defined in [Section 2.2.1](#)):

$$288 \quad g(x) = e^{-0.5 \left[\frac{(x - k_{\beta=0.5})}{(k_{\beta=0.9} - k_{\beta=0.1})/2.5} \right]^2} \quad (7)$$

289 where g is the value of the Gaussian on day x . Because the day of peak burning varies spatially
290 within the state (Liu *et al* 2019b), we cannot simply impose uniform daily variability across the
291 state using our daily DM emissions. For each grid cell, the corresponding Gaussian distribution,
292 whose maximum value is 1, is multiplied by the spatially-allocated DM emissions from Step 1.
293 Finally, we iteratively nudge the gridded DM emissions until convergence such that (1) the daily
294 total of our gridded inventory matches the state-level adjusted DM emissions, and (2) the spatial
295 allocation of our gridded inventory matches that of the MODIS Terra + Aqua unadjusted FRP on
296 a seasonal basis. One caveat is that this step assumes all grid cells within each state are equally
297 obscured by clouds. With our gridded inventory, we also provide an ancillary dataset of gridded
298 hourly fractions of fire activity, based on household survey data ([Supplementary Section S3.3](#),
299 [Figure S3](#)).

300 2.5 Ground and satellite-based measurements of aerosols

301 We use ground and satellite-based measurements of aerosols to check whether we
302 improve the temporal distribution of fire emissions over current global inventories. We focus on
303 October-November 2017, when a hazy/cloudy period lasted for almost 3 weeks during the post-
304 monsoon fire season. The Aerosol Robotic Network (AERONET) site in Kanpur, India
305 (26.51°N , 80.23°E) provides a long record of ground-based aerosol optical depth (AOD)
306 measurements (from 2001-present), which have been used to infer the properties and transport of
307 smoke aerosols emitted from post-monsoon agricultural fires across the IGP (Kaskaoutis *et al*
308 2014). As an ancillary dataset, we use the Aerosol Index (AI) from the Ozone Measuring
309 Instrument (OMI) aboard the Aura satellite, gridded to a spatial resolution of $1^\circ \times 1^\circ$. The OMI
310 AI reliably indicates enhancements in absorbing aerosols, such as those in soot and smoke, using
311 radiances at the 354 and 388-nm ultraviolet wavelengths (Torres *et al* 2007, Kaskaoutis *et al*
312 2014). We spatially average daily AI over Punjab but exclude those days with only one
313 observation across the state.

314 3. Results and Discussion

315 3.1 Crop residue burning across the Indo-Gangetic Plain: drivers, consequences, and farmer

316 *perceptions*

317 **Figure 3** shows the average temporal evolution of fire activity, crop phenology, and
318 rainfall in Punjab, Haryana, UP, and Bihar derived from satellite data. The total post-monsoon
319 fire intensity in Punjab is on average one to two orders of magnitude higher than that in Haryana,
320 UP, and Bihar. Punjab is a highly productive state with larger fields and higher use of combine
321 harvesters, thereby yielding more excess residues that need to be managed. As shown by the
322 NBR time series, the lower maximum winter greenness in eastern IGP (0.42-0.48) compared to
323 western IGP (0.62-0.68) confirms the gap in winter crop production and yield between these two
324 regions (Jain *et al* 2017); maximum monsoon greenness is more homogenous across all states
325 (0.5-0.62). In the western IGP, the summer monsoon follows the pre-monsoon fire season from
326 March to May and precedes the post-monsoon fire season from October to December. In the
327 eastern IGP, the pre-monsoon fire season follows the earlier monsoon onset and thus starts in
328 mid-March rather than mid-to-late April. As the monsoon continues through October, the post-
329 monsoon fire season occurs later and extends to December.

330 Traditionally, farmers across the IGP have harvested rice in the post-monsoon season
331 manually. By 2017, 61-71% of households surveyed in UP and Bihar still followed this practice,
332 while 62-93% of households in Punjab and Haryana had transitioned to fully mechanized
333 harvesting, namely using combine harvesters (**Figure 4**). The large amounts of loose and intact
334 residues generated from combine harvesters are difficult to clear manually and thus often burned
335 (Tallis *et al* 2017). As crop production increases and mechanization spreads across eastern IGP,
336 burn rates will also likely increase. In 2017, over a quarter of surveyed farmers burned crop
337 residue after rice harvests, with post-monsoon fire activity concentrated in Punjab: 53% of
338 farmers in Punjab burned rice residue, compared to 9-30% in Haryana, Bihar, and UP (**Figure 4**).
339 At the household level, the year-to-year persistence in burning varies: in 2016, higher
340 percentages of farmers in Punjab (82%), Haryana (20%), and UP (14%) burned rice residue
341 compared to 2017, while a lower percentage of farmers in Bihar (18%) burned. However, the
342 decline in the burn rate in Punjab is much less pronounced (89% to 71%) when weighted by
343 operational landholding area, suggesting that farmers with larger fields continued to burn
344 residues in 2017.

345 Based on 474 responses, we find that IGP farmers started to burn rice residues as early as
346 1957, with the most rapid growth occurring after the mid-1990s (**Figure 1a**). The 10-yr period
347 with the highest rate of households adopting the practice of crop residue burning took place more
348 than a decade earlier in Punjab (mid-1990s to early 2000s) than in Haryana, Bihar, and UP (mid-
349 2000s to 2010s). The time of burning varies spatially: peak burning occurs roughly evenly
350 between mid-day (10am-2pm) and evening (2-6pm) in Punjab and Haryana but mainly in the
351 evening in UP and Bihar (**Figure 1b**). Liu *et al* (2019a) found that the method of burning also
352 varies spatially: crop residues are primarily managed by complete burning in Punjab and
353 northern Haryana and more commonly by partial burning in central and southern Haryana. This
354 conclusion is supported by the increasing fraction of partial burning from western to eastern IGP
355 (30% in Punjab to 57% in Bihar) (**Figure 1c**). Consistent with Kim Oanh *et al* (2011), we find
356 that the type of burning is associated with the method of harvest, with 68% of fields with
357 complete burns – and conversely, only 19% of those with partial burns – were harvested fully

358 mechanically in the IGP.

359 Relative to Punjab, the more recent adoption of crop residue burning at the household-
360 level in Haryana, Bihar, and UP, along with the current low rate of burning (12-46%) among
361 survey households in these states, suggests high potential growth in agricultural fire activity
362 (Figure 1a, Table S4). For example, assuming a future scenario in which all households across
363 the IGP harvest rice mechanically, the rate of crop residue burning in terms of landholding area
364 would increase by just 2-27% in Punjab and Haryana, compared to 2016-2017, but by 67-207%
365 in UP and Bihar (Table S4). These values assume that the proportion of burned versus unburned
366 fields relying on mechanized harvesting remains constant in each state.

367 Nearly 90% of farmers surveyed across the IGP believe that rice residue burning impacts
368 the air quality of nearby cities (Table S3). Nevertheless, for farmers, the positive effects of
369 burning, namely saving time and cost in rice residue management, ultimately outweigh the
370 potential negative effects, including what the farmers fear could be damages to soil health and
371 lower crop yield. We find that 56-92% farmers burn rice residue to overcome the short
372 turnaround time to prepare the land to sow the next crop (Figure S1a). Nearly three quarters of
373 households wait 10 or fewer days after rice harvests to burn the crop residue, underscoring the
374 quick transition from the *kharif* to *rabi* crops (Figure S1b). Other factors that play a role in the
375 decision to burn crop residue include the unsuitability of the rice residue as cattle feed (42-76%
376 of farmers), difficulty in cutting and managing the residue (61-80%), absence of technology to
377 manage the residue (29-64%), and lack of incentive from the government to not burn, especially
378 in Punjab, where 81% of surveyed farmers cite this factor (Figure S1a). In addition to
379 circumventing the short transition period between crops, 80% of farmers say that burning saves
380 cost in cutting and managing rice residue (Table S3). On the other hand, more farmers believe
381 that crop residue burning negatively (39-44%) rather than positively (7-29%) affects soil health
382 in terms of crop yield, fertilizer usage, and soil color and texture.

383 3.2 Adjusted emissions from agricultural fires using satellite and survey data

384 Figure 2 shows an example of daily timeseries of MODIS FRP adjusted for small fires,
385 cloud/haze gaps in satellite observations, partial burning, and the fire diurnal cycle for Punjab
386 for the 2017 post-monsoon season. The VIIRS small fires boost increases MODIS FRP on clear-
387 sky days and overall by 90%, while the cloud/haze gap fill further increases the overall MODIS
388 + VIIRS FRP by 84%, with the greatest adjustment during cloudy/hazy periods, such as from
389 October 30 to November 17 (Figure 2). The household survey data implies that partial field
390 burning adds 33% more FRP. Accounting for the fire diurnal cycle results in a further 500%
391 boost in FRP, by far the most uncertain of the adjustments. This boost is due to the large number
392 of short-lasting fires inferred from the survey data that occur outside the satellite overpass times,
393 leading to “missing,” or unobserved fire activity in this region (Liu *et al* 2019a). Our FRP
394 estimates are not sensitive to the assumption that fires last just half an hour. For example, if we
395 assume instead that fires last an hour, the 2.67 factor to account for fires seen outside the satellite
396 overpasses during mid-day survey period would be halved, and the FRP to FRE conversion
397 factor would double, thereby yielding no change in our estimate of DM burned.

398 Using the adjusted FRP, we estimate on average 10.8 ± 2.7 Tg DM burned, or 68 ± 17 Gg
399 OC, 5.8 ± 1.5 Gg BC, 821 ± 206 Gg CO, and 15.4 ± 3.9 Tg CO₂, in the IGP per post-monsoon

400 burning season from 2003-2018 (Figure 5a-b). Punjab comprises 68% of total DM burned and
401 65% of aerosol emissions. Importantly, our FRP-based estimates of DM burned calculated from
402 adjusted FRP in 2016-2017 are consistent with our bottom-up estimates based on burn rates from
403 the household survey and Indiastat and IPCC fuel loadings (Figure 6a). Overall, DM burned
404 increased by 84% from 2003 to 2018. In contrast, without adjustment, the apparent 16% increase
405 in MODIS Terra + Aqua FRP is not statistically significant. The discrepancy in trends arises
406 because as fire intensity increases, haze cover also likely increases and obscures fires at a higher
407 rate. Our cloud/haze gap fill compensates for the ~28% decline in the satellite observable
408 fraction (Figure S2b), contributing on average more than twice as much FRP boost in later years
409 (2013-2018) than in previous years (2003-2012).

410 Figure 6b compares the 2003-2018 timeseries of OC+BC emissions from this study to
411 five global fire emissions inventories during the post-monsoon season. The average seasonal
412 OC+BC emissions can differ by > 90 Gg between the minimum (GFASv1.2, GFEDv4s) and
413 maximum (FEERv1-G1.2) values. Our estimates are closest in magnitude to FINNv1.5, higher
414 than GFEDv4s, GFASv1.2, and QFEDv2.5r1 but lower than FEERv1-G1.2.

415 To further examine the utility of our adjusted FRP approach, we compare our daily DM
416 burned with different global inventories in the context of aerosol loading in Punjab from
417 October-November 2017 (Figure 7). In 2017, an almost 3-week cloudy/hazy period persisted
418 from October 30 to November 17, with minimal fire activity detected during the second and third
419 weeks of November. Using a model combined with satellite data, Dekker *et al* (2019) suggested
420 that residential and commercial combustion was the most important driver of extreme pollution
421 over the IGP from November 11-19, 2017. However, we argue that agricultural fire activity
422 during this period is grossly underestimated and likely also a key emissions source. Our
423 reasoning is as follows. First, three global inventories — GFASv1.2 (used in Dekker *et al*
424 (2018)), FINNv1.5, and QFEDv2.5r1 — all show a hiatus in fire activity bounded by two local
425 maxima in fire activity (Figure 7a-b). This hiatus coincides with the cloudy/hazy period and low
426 satellite observable fraction (mostly < 70%) during the Aqua overpass time, or when most post-
427 monsoon fires occur (Figure 7b; Vadrevu *et al* 2011). Second, the variations in aerosol loading
428 during this time period closely follow the Gaussian-like temporal evolution expected of post-
429 monsoon fires (Figure 7c; Kaskaoutis *et al* 2014, Liu *et al* 2019b). Enhancements in both daily
430 AOD (> 1) at Kanpur and mean OMI AI (> 1.5) over Punjab throughout the cloudy/hazy period
431 suggest that fire activity continued during this time although obscured from satellite detection.

432 While GFASv1.2 and QFEDv2.5r1 include cloud correction algorithms to account for
433 observation gaps (Kaiser *et al* 2012, Darmenov and da Silva 2013), our study demonstrates that
434 more rigorous correction is needed during persistent cloudy/hazy conditions. We iteratively gap
435 fill this hiatus in observed FRP in 2017, resulting in daily DM burned that follows a Gaussian-
436 like distribution similar to that in other years, and more closely matches the bottom-up approach
437 based on the household survey burn rates and Indiastat rice production (Figure 7a; Liu *et al*,
438 2019b). However, the 13-37% underestimate of DM burned in 2017 using our FRP-based
439 approach compared to the bottom-up method suggests that our cloud/haze gap fill adjustments to
440 MODIS FRP may still be somewhat conservative (Figure 6).

441 *3.2.1. Limitations and uncertainties in constructing spatio-temporal explicit emissions*

442 **Figure 5c** shows average total DM burned from 2003-2018 over the IGP from our
443 gridded $0.25^\circ \times 0.25^\circ$ inventory. While our adjusted FRP approach leads to a more realistic
444 seasonal, state-level budget for DM emissions than current global inventories, we note several
445 limitations. First, the disaggregated emissions inventory contains statistical noise from the
446 iterative cloud/haze gap adjustments and our assumption that the temporal distribution of
447 emissions is Gaussian within each grid cell. Further analysis using AOD observations with back
448 trajectory modeling could help to constrain the daily variability in fire emissions. Second, the
449 household survey sample sizes for Haryana, UP, and Bihar are only 10-29% of that for Punjab,
450 leading to uncertainty in the implications of the survey for these states (**Figure 1**). While we are
451 confident in the survey-derived partial burn and fire diurnal cycle fractions for Punjab, the burn
452 rate used for validation is more uncertain, given that recent bans on agricultural burning in
453 Punjab may have led to underreporting. Third, we adjust FRP to account for the fire diurnal cycle
454 and partial fields burns by assuming a uniform spatial and temporal distribution across each
455 state. More detailed on-the-ground data may help to constrain the spatio-temporal variability in
456 these two parameters. Fourth, as with current global fire emissions inventories, we lack
457 information to provide detailed uncertainty estimates for our gridded emissions. Thus far, only
458 the emissions factors for different species allow for a detailed uncertainty analysis based on
459 standard deviations from the laboratory and field studies compiled by Andreae (2019) and Lasko
460 and Vadrevu (2018).

461 In our adjusted FRP approach, the fraction of cloud/haze gap-fill FRP to satellite-
462 observed FRP can be taken as the relative uncertainty of satellite-derived FRP from year to year
463 (**Figure S4**). This uncertainty anti-correlates with the satellite observable fraction (**Figure S2b**).
464 A further 5-9% uncertainty stems from the static VIIRS FRP boost factor applied to years from
465 2003-2011, when no VIIRS observations are available (**Table S7**). For the survey-based
466 components, we use a bootstrap hold-out method to estimate 10-18% uncertainty in partial burn
467 fractions and 14-42% in the diurnal cycle boost for the four states (**Table S8**).

468 *3.3 Differences in fire activity, fuel consumption, and emissions factors assumed in inventories*
469 *and the consequences for emissions estimates*

470 Global fire emissions inventories ingest different combinations of MODIS burned area
471 and active fire products. For example, GFEDv4s, a bottom-up inventory, relies primarily on the
472 MCD64A1 burned area product with the MCD14ML active fire product for its small fire boost,
473 while GFASv1.2, QFEDv2.5r1, and FEERv1.0-G1.2 use FRP from the MOD/MYD14 active fire
474 products (Liu *et al* 2020). In **Figure S5**, we compare the spatial patterns of burned area
475 (MCD64A1) and active fire pixels (MxD14A1) stacked by year, in which for each pixel any
476 occurrence of burning for a given post-monsoon season is assigned a value of 1. The stacked
477 values for MCD64A1 are more spatially uneven than MxD14A1 and tend to cluster, which may
478 reflect classification bias in this product caused by the conflation of harvest and burning. This
479 conflation becomes especially problematic as rice production increases (Liu *et al* 2019b),
480 because the greater drawdown in satellite-observed greenness after rice maturation may
481 artificially inflate total burned area.

482 In contrast, MxD14 can capture smaller, fragmented burns but may miss fires occurring

483 outside overpass times and result in inconsistent detection from year to year. In constructing
484 GFAS, Kaiser *et al* (2012) surmised that FRP observed during the MODIS overpasses is
485 representative of daily fire activity. While this is a reasonable assumption for large wildfires, the
486 short duration of fires in north India makes this approach problematic. Some top-down
487 inventories, such as GFASv1.2, also rely on bottom-up inventories, such as GFEDv4s, to linearly
488 scale FRP to DM (Kaiser *et al* 2012). Consequently, biases in bottom-up estimates of DM
489 burned can propagate to top-down inventories.

490 The bottom-up approach to calculate DM burned mainly depends on two variables:
491 burned area and fuel consumption, which is the mass of biomass burned per unit area. We next
492 explore how the range in these two components in different datasets affects estimates of DM
493 burned and the resulting aerosol emissions for the 2003-2016 time period. We consider (1)
494 burned area estimates from GFEDv4s, FINNv1.5, and ModL2T (Liu *et al* 2019a); (2) fuel
495 consumption estimates from GFEDv4s, FINNv1.5, Indiastat, and IPCC (Table S9); and (3)
496 emissions factors used by GFEDv4s, FINNv1.0, GFASv1.0, and QFEDv2.4 (Table S10; van der
497 Werf *et al* 2017, Wiedinmyer *et al* 2011, Kaiser *et al* 2012, Darmenov and da Silva 2013), and
498 from Andreae (2019). We find that the DM burned calculated using our best estimates of burned
499 area (ModL2T) and fuel consumption (Indiastat) is consistent with the adjusted FRP approach of
500 this study (7.3 Tg) (Figure 8). This indicates that ModL2T burned area has utility for deriving
501 agricultural fire emissions, but only when paired with reasonable fuel consumption estimates.
502 The average out-of-box GFEDv4s DM burned (3.2 Tg) is 56% lower than this study, while that
503 of FINNv1.5 (7.9 Tg) is comparable. However, the FINNv1.5 fuel consumption is more than
504 twice that estimated from Indiastat and IPCC recommendation for rice residues (Table S9),
505 compensating for its 37-55% lower burned area compared to other estimates. If we apply
506 FINNv1.5 fuel consumption to GFEDv4s and ModL2T burned area, the resulting DM burned is
507 ~2-3 times as high as this study's FRP-based estimates (Figure 8).

508 We also calculate the percent contribution of burned area, fuel consumption, and
509 emissions factors to the range in OC, BC, CO, and CO₂ agricultural fire emissions. We find that
510 fuel consumption is the most uncertain component (54-66%), followed by burned area (24-29%)
511 and emissions factors (5-22%) (Table S11). We also diagnose a 16-27% decline ($p < 0.05$) in
512 GFEDv4s and FINNv1.5 fuel consumption from 2003-2016 (Table S9), while that based on
513 Indiastat is relatively constant (+3%, $p = 0.3$). Here we will focus on the fuel load component of
514 fuel consumption (see Eq. 6) since combustion completeness is not readily observable using
515 satellite data. In Indiastat, the increase in rice production implies a higher fuel load, but the
516 concurrent increase in rice area cancels out this effect. The discrepancy between the two satellite
517 products and Indiastat can be explained by assumptions in GFEDv4s and FINNv1.5 regarding
518 vegetated fraction and fuel load. First, both global inventories use satellite-derived sub-pixel-
519 level vegetated fraction to scale fire pixels such that only the vegetated fraction of each pixel
520 counts toward the total burned area. Overall, these vegetated fractions increased by 9% ($p <$
521 0.05) in Punjab from 2003-2016, consistent with the increase in rice area reported by Indiastat.
522 Second, we would also expect to see a positive trend fuel load in FINNv1.5 and GFEDv4s due to
523 the increase in rice production. However, FINNv1.5 assumes a constant fuel load for each region
524 and land cover type (Wiedinmyer *et al* 2011), while GFEDv4s models carbon fluxes to calculate
525 fire emissions at monthly time steps, using climatological fuel loads (van der Werf *et al* 2010).

526 The shift in peak burning from October to November in Punjab (Figure S6) means that a higher
527 fraction of post-monsoon burned area in GFEDv4s is multiplied by the lower fuel consumption
528 historically characteristic of this state in November.

529 Taken together, fuel consumption and the fire diurnal cycle represent two important
530 sources of uncertainty in agricultural fire emissions in global inventories. While the survey
531 constraints in this study cannot be applied globally due to the expense of conducting such
532 surveys, our work suggests that global inventories should consider satellite-derived or
533 government statistics of crop production, yield, and area to constrain fuel loads. Geostationary
534 satellite fire observations can also be useful to constrain the diurnal cycle of fire activity, where
535 such data are available.

536 **4. Conclusion**

537 In summary, we combine household survey results with satellite observations to revise
538 estimates of post-monsoon agricultural fire emissions across north India from 2003-2018. To do
539 so, we develop an approach based on MODIS FRP, adjusted for small fires from VIIRS,
540 cloud/haze gaps in satellite observations, partial-field burns, and the diurnal cycle of fire activity.
541 Regionally, we estimate average emissions of 68 Gg OC, 5.8 Gg BC, 821 Gg CO, and 15.4 Tg
542 CO₂. Our estimates of DM burned for Punjab, which contributes two-thirds of emissions, closely
543 match the bottom-up validation estimates using state-level government statistics and survey burn
544 rates from 2016 and 2017. Importantly, our cloud-gap fill leads to an 84% increase in DM
545 burned in Punjab from 2003-2018; without this adjustment, the trend in MODIS FRP is only
546 16% and not statistically significant. Here we constrain the fire diurnal cycle and fuel
547 consumption, two components that contribute most to bias and disagreement across this region
548 among standard global fire emissions inventories used in atmospheric studies. Our results
549 suggest that additional information from household surveys and crop statistics can help constrain
550 these two components. We construct a daily, 0.25° x 0.25° emissions inventory over the IGP by
551 disaggregating state-level DM burned. Our emissions inventory, SAGE-IGP, may be used with
552 atmospheric transport models to estimate smoke exposure downwind and evaluate the associated
553 public health burden and climate impacts. Potential expansion of crop residue burning among
554 smallholder farms in north India, where satellites poorly capture fire activity, makes regional,
555 survey-constrained inventories such as ours valuable for improving emissions estimates.

556 **Data Availability**

557 The CHIRPS rainfall and MODIS/VIIRS land cover, active fire, and surface reflectance datasets
558 are publicly available through Google Earth Engine (<http://earthengine.google.com/>).
559 MODIS/VIIRS datasets are freely available from NASA's Earthdata platform
560 (<https://earthdata.nasa.gov/>).

561 The gridded daily, 0.25° x 0.25° agricultural fire emissions inventory from this study (SAGE-
562 IGP) will be available from Harvard Dataverse at <https://doi.org/10.7910/DVN/JUMXOL>.

563 **Acknowledgements**

564 This work was supported by a National Science Foundation Graduate Research Fellowship
565 awarded to T. Liu. (DGE1745303). We thank the principal and co-investigators and site manager
566 for AERONET site at IIT Kanpur, India for managing data collection and processing. Survey
567 work was funded by a National Science Foundation SEES Postdoctoral Award (Award No.
568 1415436) and a NASA Land Cover and Land Use Change Grant (NNX17AH97G) awarded to
569 M. Jain. The survey was reviewed and approved by the Institutional Review Board (IRB
570 Approval Number: HUM00140594) at the University of Michigan.

571 **References**

- 572 Aalde H, Gonzalez P, Gytarsky M, Krug T, Kurz W A, Lasco R D, Martino D L, McConkey B
573 G, Ogle S, Paustian K, Raison J, Ravindranath N H, Schoene D, Smith P, Somogyi Z, van
574 Amstel A and Verchot L 2006 Chapter 2: Generic Methodologies Applicable to Multiple
575 Land-Use Categories 2006 *IPCC Guidelines for National Greenhouse Gas Inventories, Vol*
576 *4: Agriculture, Forestry, and Other Land Use*
- 577 Andreae M O 2019 Emission of trace gases and aerosols from biomass burning – An updated
578 assessment *Atmos. Chem. Phys.* **19** 8523–46 Online: <https://doi.org/10.5194/acp-2019-303>
- 579 Badarinath K V S, Kharol S K and Sharma A R 2009 Long-range transport of aerosols from
580 agriculture crop residue burning in Indo-Gangetic Plains-A study using LIDAR, ground
581 measurements and satellite data *J. Atmos. Solar-Terrestrial Phys.* **71** 112–20
- 582 Badarinath K V S, Kiran Chand T R and Krishna Prasad V 2006 Agriculture crop residue
583 burning in the Indo-Gangetic Plains - A study using IRS-P6 AWiFS satellite data *Curr. Sci.*
584 **91** 1085–9
- 585 Bikkina S, Andersson A, Kirillova E N, Holmstrand H, Tiwari S, Srivastava A K, Bisht D S and
586 Gustafsson Ö 2019 Air quality in megacity Delhi affected by countryside biomass burning
587 *Nat. Sustain.* Online: <https://doi.org/10.1038/s41893-019-0219-0>
- 588 Burney J and Ramanathan V 2014 Recent climate and air pollution impacts on Indian agriculture
589 *Proc. Natl. Acad. Sci.* **111** 16319–24 Online: <https://doi.org/10.1073/pnas.1317275111>
- 590 Chakrabarti S, Khan M T, Kishore A, Roy D and Scott S P 2019 Risk of acute respiratory
591 infection from crop burning in India: estimating disease burden and economic welfare from
592 satellite and national health survey data for 250 000 persons *Int. J. Epidemiol.* 1–12 Online:
593 <https://doi.org/10.1093/ije/dyz022>
- 594 Cusworth D H, Mickley L J, Sulprizio M P, Liu T, Marlier M E, DeFries R S, Guttikunda S K
595 and Gupta P 2018 Quantifying the influence of agricultural fires in northwest India on urban
596 air pollution in Delhi, India *Environ. Res. Lett.* **13** 044018 Online:
597 <https://doi.org/10.1088/1748-9326/aab303>
- 598 Darnenov A S and da Silva A 2013 *The Quick Fire Emissions Dataset (QFED) -*
599 *Documentation of versions 2.1, 2.2, and 2.4* vol 32, ed M J Suarez Online:
600 <http://citeseerx.ist.psu.edu/viewdoc/summary?doi=10.1.1.406.7724>
- 601 Dekker I N, Houweling S, Pandey S, Krol M, Röckmann T, Borsdorff T, Landgraf J and Aben I
602 2019 What caused the extreme CO concentrations during the 2017 high pollution episode in

- 603 India? *Atmos. Chem. Phys.* **19** 3433–45 Online: <https://doi.org/10.5194/acp-2018-1061>
- 604 Ghude S D, Jena C K, Beig G, Kumar R, Kulkarni S H and Chate D M 2016 Impact of emission
605 mitigation on ozone-induced wheat and rice damage in India *Curr. Sci.* **110** 1452–8 Online:
606 <https://doi.org/10.18520/cs/v110/i8/1452-1458>
- 607 Gorelick N, Hancher M, Dixon M, Ilyushchenko S, Thau D and Moore R 2017 Google Earth
608 Engine: Planetary-scale geospatial analysis for everyone *Remote Sens. Environ.* **202** 18–27
609 Online: <https://doi.org/10.1016/j.rse.2017.06.031>
- 610 Gupta R 2012 *Causes of Emissions from Agricultural Residue Burning in North-West India:
611 Evaluation of a Technology Policy Response* Online:
612 http://www.sandeeonline.org/uploads/documents/publication/962_PUB_Working_Paper_66
613 [_Ridhima_Gupta.pdf](http://www.sandeeonline.org/uploads/documents/publication/962_PUB_Working_Paper_66_Ridhima_Gupta.pdf)
- 614 Ichoku C and Ellison L 2014 Global top-down smoke-aerosol emissions estimation using
615 satellite fire radiative power measurements *Atmos. Chem. Phys.* **14** 6643–67 Online:
616 <https://doi.org/10.5194/acp-14-6643-2014>
- 617 Jain M, Singh B, Srivastava A A K, Malik R K, McDonald A J and Lobell D B 2017 Using
618 satellite data to identify the causes of and potential solutions for yield gaps in India's Wheat
619 Belt *Environ. Res. Lett.* **12** 094011
- 620 Jethva H, Chand D, Torres O, Gupta P, Lyapustin A and Patadia F 2018 Agricultural Burning
621 and Air Quality over Northern India: A Synergistic Analysis using NASA's A-train Satellite
622 Data and Ground Measurements *Aerosol Air Qual. Res.* **18** 1756–73 Online:
623 <http://doi.org/10.4209/aaqr.2017.12.0583>
- 624 Kaiser J W, Andela N, Atherton J, de Jong M, Heil A, Paugam R, Remy S, Schultz M G, van der
625 Werf G R, van Leeuwen T T and Wooster M J 2014 *Recommended Fire Emission Service
626 Enhancements* Online: [https://www.ecmwf.int/sites/default/files/elibrary/2014/10376-](https://www.ecmwf.int/sites/default/files/elibrary/2014/10376-recommended-fire-emission-service-enhancements.pdf)
627 [recommended-fire-emission-service-enhancements.pdf](https://www.ecmwf.int/sites/default/files/elibrary/2014/10376-recommended-fire-emission-service-enhancements.pdf)
- 628 Kaiser J W, Heil A, Andreae M O, Benedetti A, Chubarova N, Jones L, Morcrette J J, Razinger
629 M, Schultz M G, Suttie M and van der Werf G R 2012 Biomass burning emissions
630 estimated with a global fire assimilation system based on observed fire radiative power
631 *Biogeosciences* **9** 527–54 Online: <https://doi.org/10.5194/bg-9-527-2012>
- 632 Kaskaoutis D G, Kumar S, Sharma D, Singh R P, Kharol S K, Sharma M, Singh A K, Singh S,
633 Singh A and Singh D 2014 Effects of crop residue burning on aerosol properties, plume
634 characteristics, and long-range transport over northern India *J. Geophys. Res. Atmos.* **119**
635 5424–44 Online: <https://doi.org/10.1002/2013JD021357>
- 636 Kim Oanh N T, Ly B T, Tipayarom D, Manandhar B R, Prapat P, Simpson C D and Sally Liu L
637 J 2011 Characterization of particulate matter emission from open burning of rice straw
638 *Atmos. Environ.* **45** 493–502 Online: <https://doi.org/10.1016/j.atmosenv.2010.09.023>
- 639 Kumar P, Kumar S and Joshi L 2015 *Socioeconomic and Environmental Implications of
640 Agricultural Residue Burning: A Case Study of Punjab, India* Online:
641 <https://doi.org/10.1007/978-81-322-2014-5>
- 642 Lasko K and Vadrevu K 2018 Improved rice residue burning emissions estimates: Accounting
643 for practice-specific emission factors in air pollution assessments of Vietnam *Environ.*

- 644 *Pollut.* **236** 795–806 Online: <https://doi.org/10.1016/j.envpol.2018.01.098>
- 645 Liu M, Song Y, Yao H, Kang Y, Li M, Huang X and Hu M 2015 Estimating emissions from
646 agricultural fires in the North China Plain based on MODIS fire radiative power *Atmos.*
647 *Environ.* **112** 326–34 Online: <https://doi.org/10.1016/j.atmosenv.2015.04.058>
- 648 Liu T, Marlier M E, DeFries R S, Westervelt D M, Xia K R, Fiore A M, Mickley L J, Cusworth
649 D H and Milly G 2018 Seasonal impact of regional outdoor biomass burning on air
650 pollution in three Indian cities: Delhi, Bengaluru, and Pune *Atmos. Environ.* **172** 83–92
651 Online: <https://doi.org/10.1016/j.atmosenv.2017.10.024>
- 652 Liu T, Marlier M E, Karambelas A, Jain M, Singh S, Singh M K, Gautam R and DeFries R S
653 2019a Missing emissions from post-monsoon agricultural fires in northwestern India:
654 regional limitations of MODIS burned area and active fire products *Environ. Res. Commun.*
655 **1** 011007 Online: <https://doi.org/10.1088/2515-7620/ab056c>
- 656 Liu T, Mickley L J, Gautam R, Singh M K, DeFries R S and Marlier M E 2019b Detection of
657 delay in post-monsoon agricultural burning across Punjab, India: potential drivers and
658 consequences for air quality *Environ. Res. Lett.* Online:
659 <https://doi.org/10.31223/osf.io/nh5w7>
- 660 Liu T, Mickley L J, Marlier M E, DeFries R S, Khan M F, Latif M T and Karambelas A 2020
661 Diagnosing spatial biases and uncertainties in global fire emissions inventories: Indonesia
662 as regional case study *Remote Sens. Environ.* **237** 111557 Online:
663 <https://doi.org/10.1016/j.rse.2019.111557>
- 664 Mahajan G, Bharaj T S and Timsina J 2009 Yield and water productivity of rice as affected by
665 time of transplanting in Punjab, India *Agric. Water Manag.* **96** 525–32 Online:
666 <https://doi.org/10.1016/j.agwat.2008.09.027>
- 667 Palanisami K, Kakumanu K R, Nagothu U S and Ranganathan C R 2019 *Climate Change and*
668 *Future Rice Production in India: A Cross Country Study of Major Rice Growing States of*
669 *India* (Springer Singapore) Online: <https://doi.org/10.1007/978-981-13-8363-2>
- 670 Palinkas L A, Horwitz S M, Green C A, Wisdom J P, Duan N and Hoagwood K 2015 Purposeful
671 sampling for qualitative data collection and analysis in mixed method implementation
672 research Lawrence *Adm. Policy Ment. Heal. Ment. Heal. Serv. Res.* **42** 533–44 Online:
673 <https://doi.org/10.1007/s10488-013-0528-y>
- 674 Sarkar S, Singh R P and Chauhan A 2018 Crop Residue Burning in Northern India: Increasing
675 Threat to Greater India *J. Geophys. Res. Atmos.* **123** 6920–34 Online:
676 <https://doi.org/10.1029/2018JD028428>
- 677 Shyamsundar P, Springer N P, Tallis H, Polasky S, Jat M L, Sidhu H S, Krishnapriya P P, Skiba
678 N, Ginn W, Ahuja V, Cummins J, Datta I, Dholakia H H, Dixon J, Gerard B, Gupta R,
679 Hellmann J, Jadhav A, Jat H S, Keil A, Ladha J K, Lopez-Ridaura S, Nandrajog S P, Paul S,
680 Ritter A, Sharma P C, Singh R, Singh D and Somanathan R 2019 Fields on fire:
681 Alternatives to crop residue burning in India *Science (80-.).* **365** 536–8 Online:
682 <https://doi.org/10.1126/science.aaw4085>
- 683 Sidhu H S, Singh M, Yadvinder S, Blackwell J, Lohan S K, Humphreys E, Jat M L, Singh V and
684 Singh S 2015 Development and evaluation of the Turbo Happy Seeder for sowing wheat
685 into heavy rice residues in NW India *F. Crop. Res.* **184** 201–12 Online:

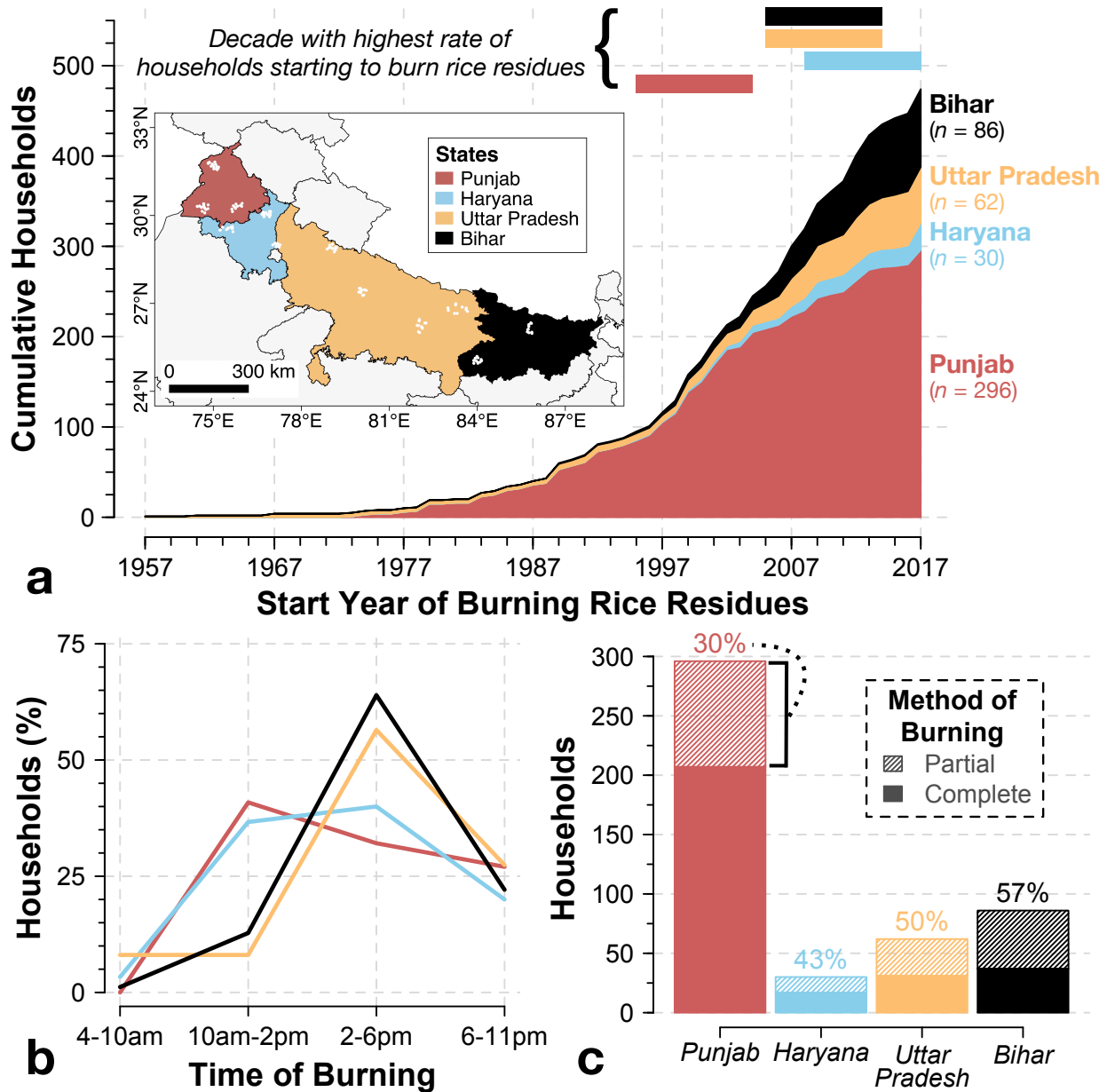
- 686 <https://doi.org/10.1016/j.fcr.2015.07.025>
- 687 Singh N J, Kudrat M, Jain K and Pandey K 2011 Cropping pattern of Uttar Pradesh using IRS-
688 P6 (AWiFS) data *Int. J. Remote Sens.* **32** 4511–26 Online:
689 <https://doi.org/10.1080/01431161.2010.489061>
- 690 Sinha B, Singh Sangwan K, Maurya Y, Kumar V, Sarkar C, Chandra B P and Sinha V 2015
691 Assessment of crop yield losses in Punjab and Haryana using 2 years of continuous in situ
692 ozone measurements *Atmos. Chem. Phys.* **15** 9555–76
- 693 Tallis H, Polasky S, Shyamsundar P, Springer N, Ahuja V, Cummins J, Datta I, Dixon J, Gerard
694 B, Ginn W, Gupta R, Jadhav A, Jat M, Keil A, Krishnapriya P, Ladha J, Nandrajog S, Paul
695 S, Lopez Ridaura S, Ritter A, Sidhu H, Skiba N and Somanathan R 2017 *The Evergreen
696 Revolution: Six Ways to empower India's no-burn agricultural future* Online:
697 <https://www.nature.org/science-in-action/the-evergreen-revolution.pdf>
- 698 Thumaty K C, Rodda S R, Singhal J, Gopalakrishnan R, Jha C S, Parsi G D and Dadhwal V K
699 2015 Spatio-temporal characterization of agriculture residue burning in Punjab and
700 Haryana, India, using MODIS and Suomi NPP VIIRS data *Curr. Sci.* **109** 1850–5 Online:
701 <https://doi.org/10.18520/v109/i10/1850-1855>
- 702 Torres O, Tanskanen A, Veihelmann B, Ahn C, Braak R, Bhartia P K, Veeffkind P and Levelt P
703 2007 Aerosols and surface UV products from Ozone Monitoring Instrument observations:
704 An overview *J. Geophys. Res. Atmos.* **112** D24S47 Online:
705 <https://doi.org/10.1029/2007JD008809>
- 706 Vadrevu K P, Csizsar I, Ellicott E, Giglio L, Badarinath K V S, Vermote E and Justice C 2013
707 Hotspot analysis of vegetation fires and intensity in the Indian region *IEEE J. Sel. Top.
708 Appl. Earth Obs. Remote Sens.* **6** 224–38 Online:
709 <https://doi.org/10.1109/JSTARS.2012.2210699>
- 710 Vadrevu K P, Ellicott E, Badarinath K V S and Vermote E 2011 MODIS derived fire
711 characteristics and aerosol optical depth variations during the agricultural residue burning
712 season, north India *Environ. Pollut.* **159** 1560–9 Online:
713 <https://doi.org/10.1016/j.envpol.2011.03.001>
- 714 van der Werf G R, Randerson J T, Giglio L, Collatz G J, Mu M, Kasibhatla P S, Morton D C,
715 Defries R S, Jin Y and Van Leeuwen T T 2010 Global fire emissions and the contribution of
716 deforestation, savanna, forest, agricultural, and peat fires (1997-2009) *Atmos. Chem. Phys.*
717 **10** 11707–35 Online: <https://doi.org/10.5194/acp-10-11707-2010>
- 718 van der Werf G R, Randerson J T, Giglio L, van Leeuwen T T, Chen Y, Rogers B M, Mu M, van
719 Marle M J E, Morton D C, Collatz G J, Yokelson R J and Kasibhatla P S 2017 Global fire
720 emissions estimates during 1997–2016 *Earth Syst. Sci. Data* **9** 697–720 Online:
721 <https://doi.org/10.5194/essd-9-697-2017>
- 722 Wiedinmyer C, Akagi S K, Yokelson R J, Emmons L K, Orlando J J and Soja A J 2011 The Fire
723 INventory from NCAR (FINN): a high resolution global model to estimate the emissions
724 from open burning *Geosci. Model Dev.* **4** 625–41 Online: [https://doi.org/10.5194/gmd-4-
725 625-2011](https://doi.org/10.5194/gmd-4-625-2011)
- 726 Wiedinmyer C, Yokelson R J and Gullett B K 2014 Global emissions of trace gases, particulate
727 matter, and hazardous air pollutants from open burning of domestic waste *Environ. Sci.*

728 *Technol.* **48** 9523–30

729 Wooster M J, Roberts G, Perry G L W and Kaufman Y J 2005 Retrieval of biomass combustion
730 rates and totals from fire radiative power observations: FRP derivation and calibration
731 relationships between biomass consumption and fire radiative energy release *J. Geophys.*
732 *Res. Atmos.* **110** D24311 Online: <https://doi.org/10.1029/2005JD006318>

733 Zhang X, Kondragunta S and Roy D P 2014 Interannual variation in biomass burning and fire
734 seasonality derived from geostationary satellite data across the contiguous United States
735 from 1995 to 2011 *J. Geophys. Res. Biogeosciences* **119** 1147–62 Online:
736 <https://doi.org/10.1002/2013JG002518>

737



738

739

740 **Figure 1. Temporal and methodological characteristics of rice residue burning across the**

741 **Indo-Gangetic Plain, inferred from household survey data for the 2017-18 growing season:**

742 **(a)** Cumulative distribution of number of households burning rice residues, ordered by start year

743 of burning with stacked contours representing contributions of four different states. The colored

744 bars at top denote the 10-yr period for each state with the highest rate of households starting to

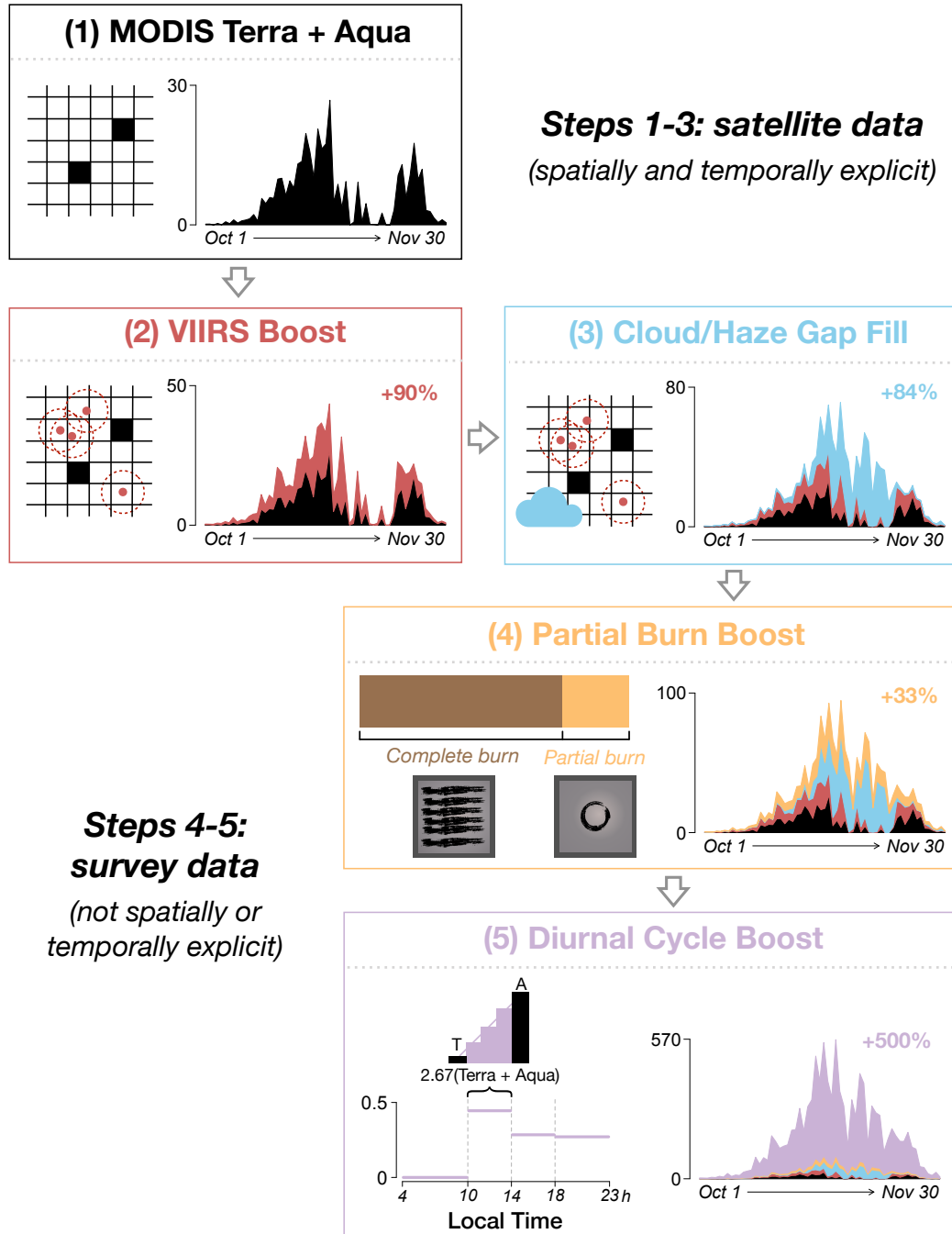
745 burn rice residues. White dots in inset panel show the locations of surveyed households that

746 harvested rice in the four states (Punjab, Haryana, Uttar Pradesh, and Bihar). **(b)** Diurnal cycle of

747 rice residue burning from early morning to late night, color coded by state. **(c)** Method of

748 burning rice residues, separated into complete and partial burning of fields. Percentages represent

the fraction of households that use partial burning.



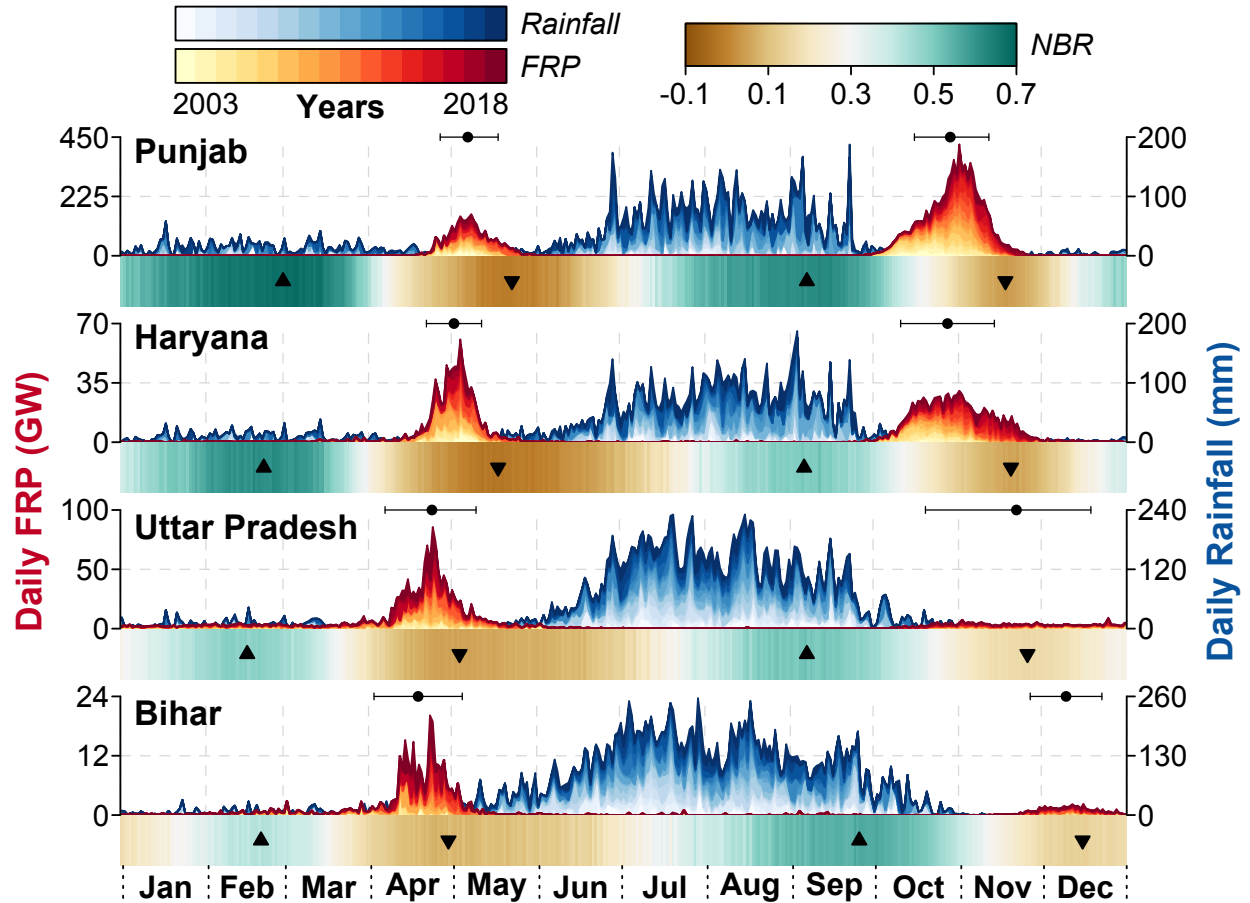
749

750 **Figure 2. Pictorial flowchart for FRP adjustments using satellite and survey data for**
 751 **Punjab in the sample year 2017:** The units for the daily FRP timeseries is GW. Percentages
 752 denote the FRP increase relative to the previous step. Checkerboards in Steps 1-3 denote a 1-km
 753 grid with MODIS FRP observations in black, VIIRS hotspots with a 1-km buffer in red, and
 754 clouds/haze cover in blue. Squares in Step 4 show the difference between complete versus partial
 755 burns, where black striations depict burning within the field. In Step 5, the plot on the left shows
 756 the diurnal cycle of fire activity, with horizontal lines showing the survey fractions (same as
 757 **Figure 1b** but weighted by landholding area) and vertical bars depicting our adjustment of mid-
 758 day satellite FRP. Detailed methods for each step are described in **Section 2.4.1**.

759 **Table 1.** Parameters for estimates of agricultural fire emissions based on burned area, active fire
760 area, and Fire Radiative Power (FRP).

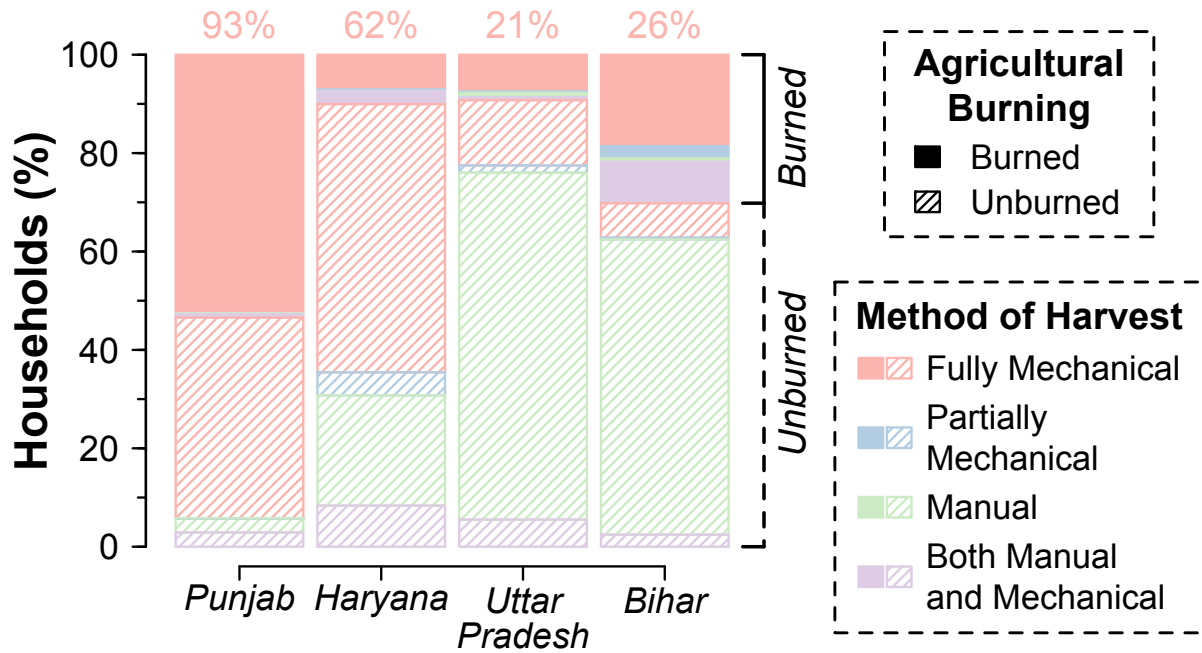
Parameter	Description	Value	Units	Source
FRE	Fire Radiative Energy	<i>varies</i>	MJ	Derived from MODIS FRP
α	Conversion factor from FRE to dry matter burned	0.41	kg MJ ⁻¹	Kaiser <i>et al</i> (2014)
f_{burned}	Fraction of rice residues burned	<i>varies</i>	unitless	Derived from survey data
CP	Crop production (<i>rice</i>)	<i>varies</i>	kg	Indiastat
A	Area cultivated (<i>rice</i>)	<i>varies</i>	m ²	Indiastat
RC	Residue to crop ratio (<i>rice</i>)	1.4-1.8	unitless	Bouwman <i>et al</i> (2000); Ravindranath <i>et al</i> (2005); Jain <i>et al</i> (2014)
f_{DM}	Mass fraction of dry matter burned from total rice production	0.82-0.88	unitless	Bouwman <i>et al</i> (2000); Jain <i>et al</i> (2014)
f_{CC}	Combustion completeness	0.89 (CB), 0.67 (PB)	unitless	Lasko & Vadrevu (2018)
EF	Emissions factor	e.g. 4.9 (OC), 0.42 (BC)	g species kg ⁻¹ DM	Andreae (2019)
	PB to CB ratio for aerosol-based emissions factors	1.92	unitless	Lasko & Vadrevu (2018)

761 CB = complete burn, PB = partial burn



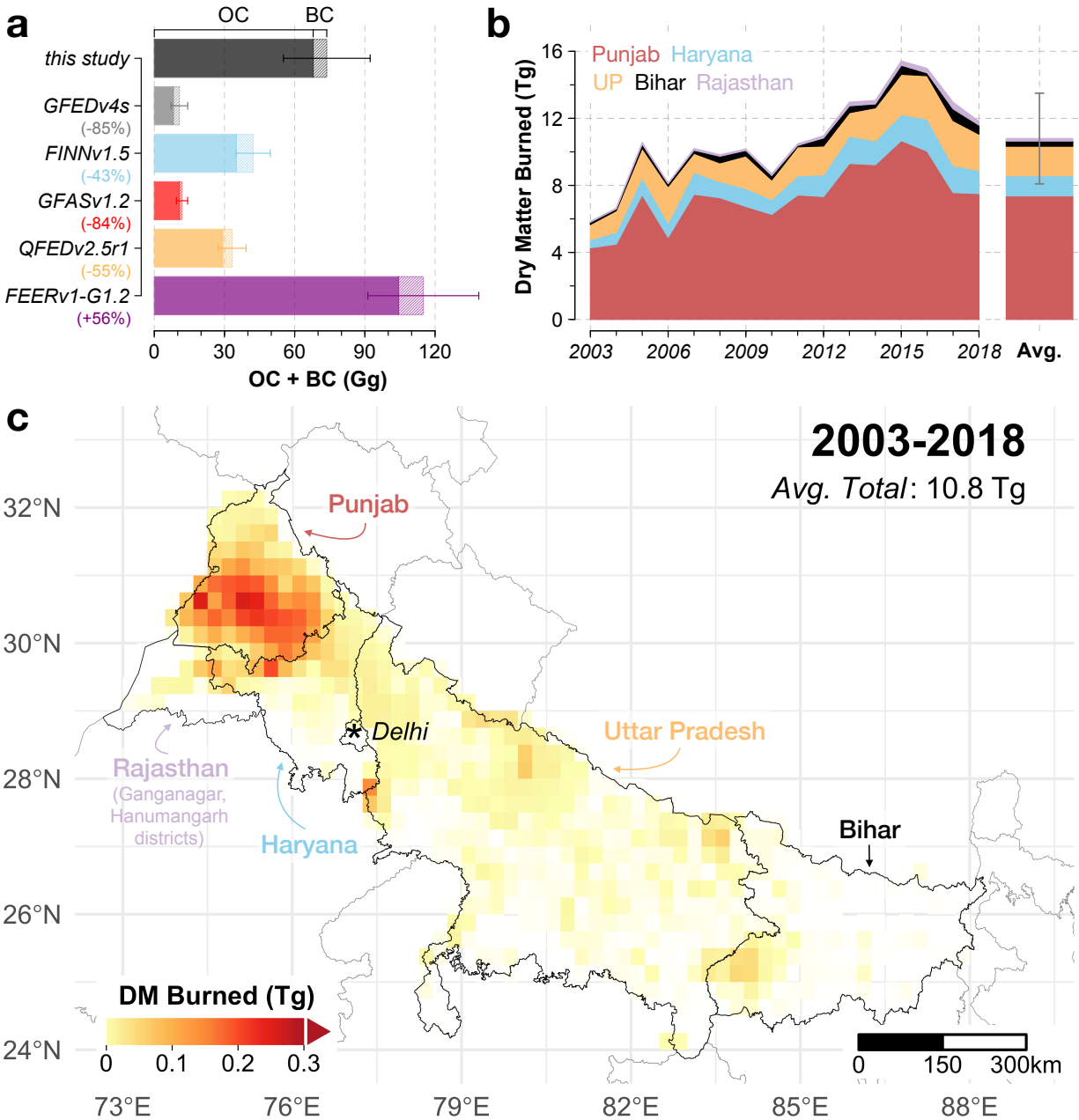
762
763
764
765
766
767
768
769
770
771
772

Figure 3. Satellite-derived daily vegetation greenness, fire intensity, and rainfall in Punjab, Haryana, Uttar Pradesh, and Bihar from 2003-2018: The Normalized Burn Ratio (NBR), a proxy for vegetation greenness, and Fire Radiative Power (FRP), a proxy for fire intensity, are derived from MODIS over agricultural regions. FRP and rainfall are stacked by year, while NBR is shown as the weighted average across all years, with weights based on the usable fraction, or fraction of agricultural area that is cloud and haze-free on that day in each year. Segmented bars denote the approximate start, midpoint, and end of the pre-monsoon (March-May) and post-monsoon (Oct-Dec) burning seasons in each state. Upward triangles denote the timing of maximum monsoon and winter greenness; conversely, downward triangles denote the timing of minimum pre-monsoon and post-monsoon greenness.

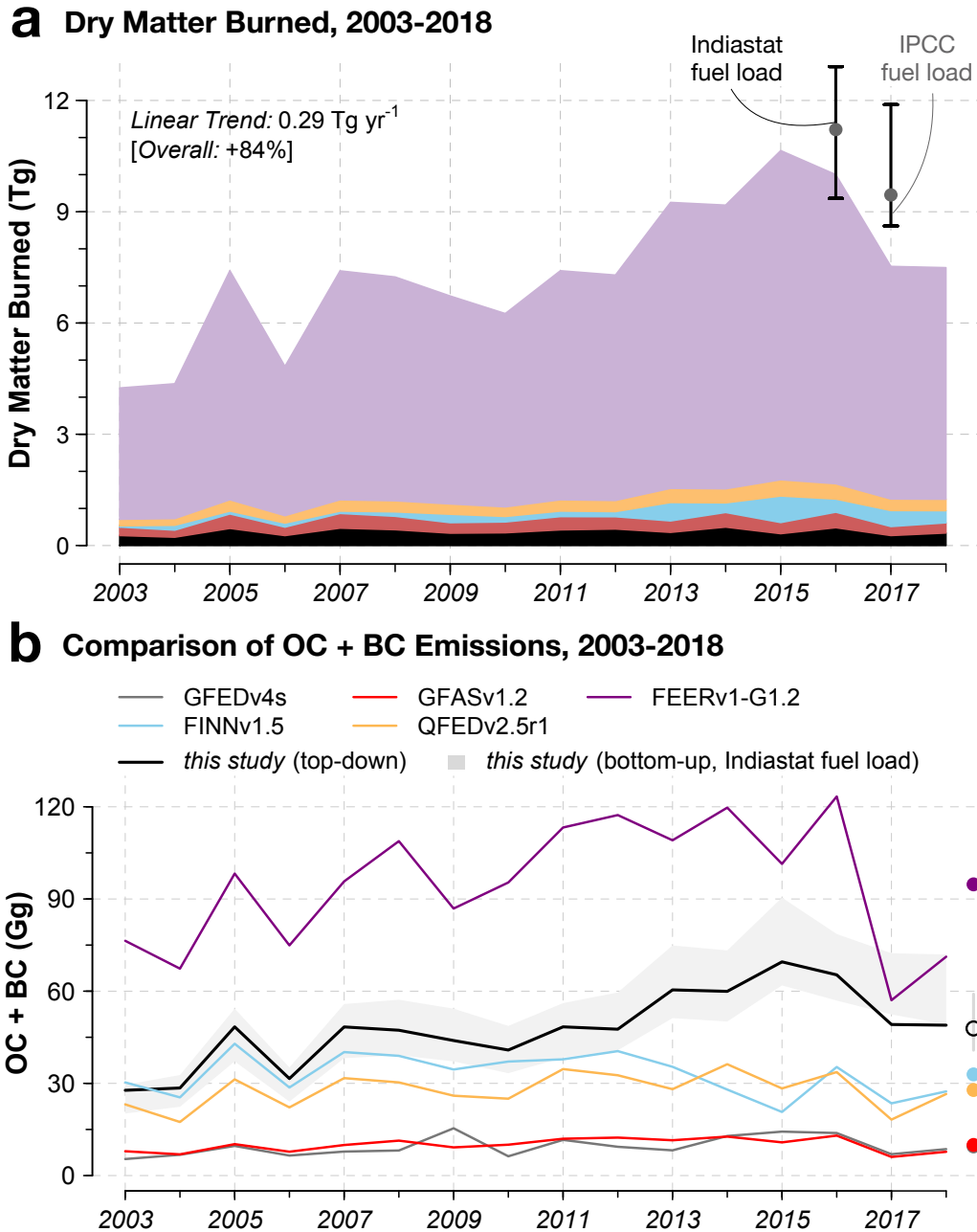


773
774
775
776
777
778

Figure 4. Mechanized harvesting of rice related to crop residue burning across the Indo-Gangetic Plain inferred from household survey data: The percentage of households that burned and did not burn rice residues, separated by the method of harvest, for the 2017-18 growing season. Percentages above bars denote the fraction of households using fully mechanical methods (combine harvesters) to harvest *kharif* rice.

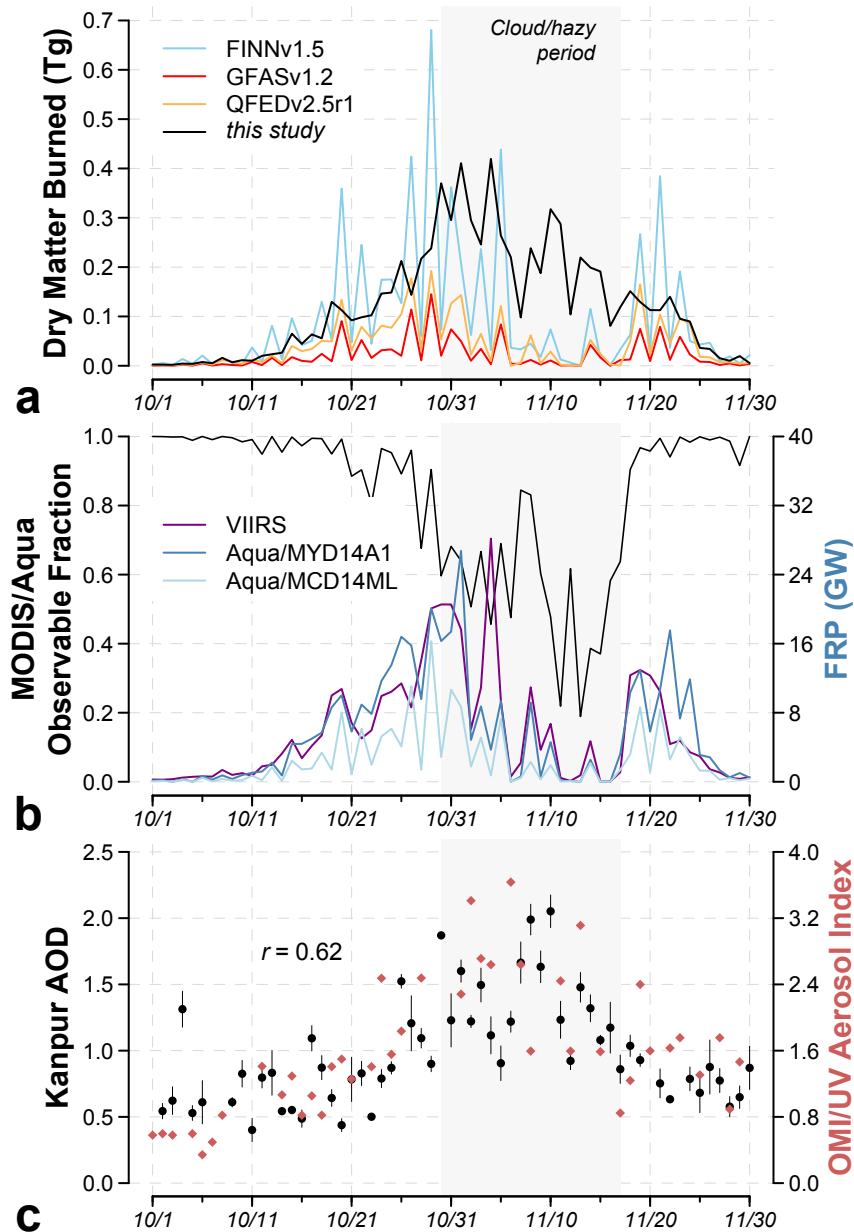


779
 780 **Figure 5. Post-monsoon agricultural fire emissions over the IGP from 2003-2018: (a)**
 781 Comparison of average OC+BC emissions ($\pm 1\sigma$) from this study (SAGE-IGP) with five global
 782 fire emissions inventories. On the y-axis, percentages denote the difference in OC+BC emissions
 783 from each inventory relative to this study. (b) Time series of annual dry matter (DM) burned, and
 784 average DM burned from 2003-2018, with stacked contours showing contributions by state.
 785 Vertical bars denote $\pm 1\sigma$ for the total DM burned across all years. (c) Average state-level DM
 786 burned in Punjab, Haryana, Uttar Pradesh, and Bihar, disaggregated to $0.25^\circ \times 0.25^\circ$ spatial
 787 resolution using the top-down adjusted FRP approach from this study. DM burned is also
 788 estimated for two Rajasthan districts, Ganganagar and Hanumangarh, which border Punjab and
 789 Haryana. Inset shows the average total DM burned from 2003-2018.

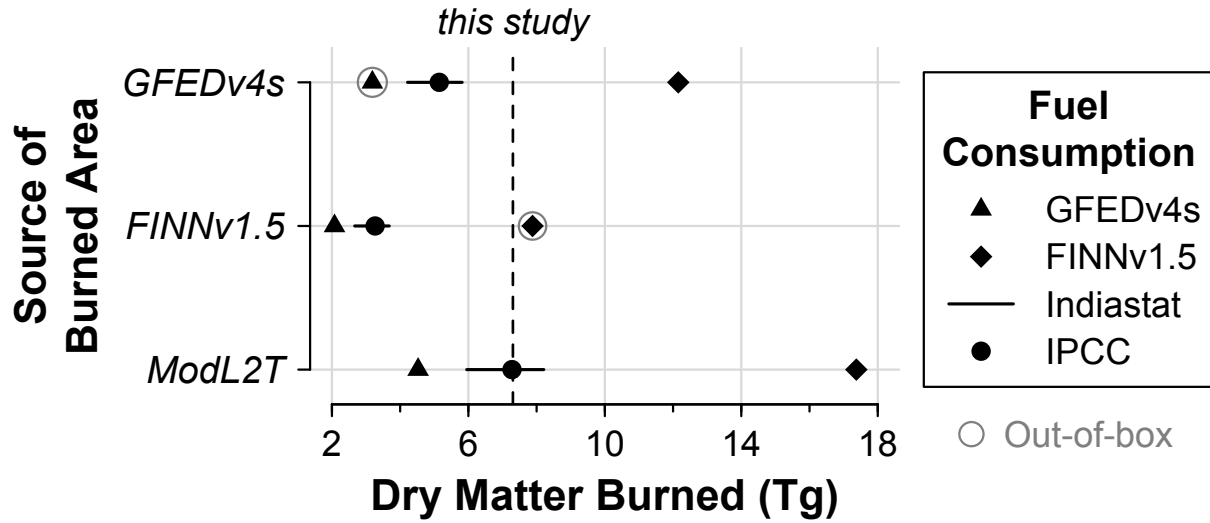


790

791 **Figure 6. Dry matter (DM) burned from adjusted FRP and comparison of OC+BC**
 792 **emissions for Punjab, India, from 2003-2018: (a)** Post-monsoon DM burned (Tg), derived
 793 using an FRP-based approach with both satellite and survey data. Stacked colored contours
 794 represent the FRP adjustments illustrated in Figure 2. Black bars (Indiastat) and gray dots (IPCC)
 795 denote the range of post-monsoon DM burned derived using a bottom-up approach with survey
 796 data for 2016 and 2017. (b) Comparison of post-monsoon OC+BC emissions from this study and
 797 five global fire emissions inventories. Dots on the right show average OC+BC emissions for this
 798 study and all inventories. The gray envelope for this study's bottom-up estimate denotes ranges
 799 in the residue-to-crop ratio and fraction of DM burned tuned to 2016-17 survey burn rates (see
 800 Table 1), and the gray bar at right shows the average across years.



801
 802 **Figure 7. Daily fire emissions and intensity in Punjab, India, and aerosols observed over**
 803 **Punjab and in Kanpur, India, during the 2017 post-monsoon burning period: (a)** DM
 804 burned from this study and three fire emissions inventories: GFASv1.2, QFEDv2.5r1, and
 805 FINNv1.5. **(b)** Fire intensity as measured by FRP from MODIS/Aqua (MYD14A1 gridded
 806 maximum FRP and MCD14ML FRP from individual active fire hotspots) and from VIIRS
 807 (VNP14IMGML), overlaid with the MODIS/Aqua “observable fraction” f_o , or the degree to
 808 which MODIS/Aqua can “see” active fires. The cloudy/hazy period from October 30 to
 809 November 17 is highlighted in light gray. **(c)** Daily mean AOD ($\pm 1\sigma$) at 500 nm from the
 810 AERONET site in Kanpur (black) and OMI/UV Aerosol Index (AI, red) over Punjab. The
 811 correlation r between the AOD and AI timeseries is shown inset.



812

813

814

815

816

817

818

819

Figure 8. Comparison of average dry matter (DM) burned derived from different combinations of bottom-up burned area and fuel consumption estimates for the 2003-2016 post-monsoon burning seasons in Punjab, India: Three sources of burned area (GFEDv4s, FINNv1.5, and ModL2T (Liu et al., 2019)) and four fuel consumption estimates (GFEDv4s, FINNv1.5, Indiastat, IPCC (2006)) provide a range of DM estimates (Tg). The out-of-box DM averages from GFEDv4s and FINNv1.5 are circled. The average DM estimated from the top-down approach developed in this study is shown as the vertical dashed line.